

# High Angular Resolution Measurement of Ion and Neutral Spectra as a Probe of the Magnetic Field Structure in DR21(OH)

Shih-Ping Lai<sup>1</sup>, T. Velusamy, and W. D. Langer

*slai@astro.umd.edu, velu@jpl.nasa.gov, william.langer@jpl.nasa.gov*

*Jet Propulsion Laboratory, California Institute of Technology, MS 169-506, 4800 Oak Grove Dr., Pasadena, CA 91109*

## ABSTRACT

It has been suggested that under average interstellar field strengths the cyclotron interaction between ions and magnetic fields is strong enough to narrow the linewidth and suppress the line wings in the ion spectra. We present evidence for the cyclotron interaction effect at arcsec scale on the velocity dispersions in the spectra of ion/neutral molecular species in DR21(OH) observed with the OVRO-MMA. Using a spatial resolution  $\sim 3$  times higher than previous CSO observations by Houde et al. (2002), we show that  $\text{H}^{13}\text{CO}^+$  and  $\text{H}^{13}\text{CN}$  are coexistent at the scale of our observations ( $6''$ ). In the eastern parts of the DR21(OH) core where the dynamics is simple, the ion linewidths are indeed narrower than the neutral linewidths with an average ion-to-neutral linewidth ratio of  $0.82 \pm 0.04$ . We use our results, along with the existing Zeeman and dust/CO polarization data on small scales, to derive the 3-D magnetic field structure. We obtain a field strength of  $0.44 \pm 0.12$  mG with inclination of  $36^\circ$  to the line of sight, directed toward the observer, and a position angle of  $-75^\circ$  in the plane of the sky. With the full magnetic field strength derived here, we are able to conclude that the MM1 core of DR21(OH) is magnetically supercritical; although turbulence provides the dominant support.

*Subject headings:* star formation, magnetic fields

## 1. Introduction

Measurements of magnetic fields in the environment of star forming regions are mostly carried out with observations of Zeeman splitting (Crutcher 1999), the polarimetry of dust

---

<sup>1</sup>Current address: Department of Astronomy, University of Maryland, College Park, MD 20742-2421

continuum (Dotson et al. 2000; Lai et al. 2001, 2002), and the polarimetry of CO emission (Girart et al. 1999; Lai et al. 2003). The Zeeman observations only give the field *strength* along the line of sight, and the polarimetry of dust continuum and CO emission yield the field *direction* in the plane of sky. As a result, these observations do not determine the full strength and orientation of the magnetic fields in 3-D. To characterize the magnetic field environment, we need to measure directly the magnetic field strength in the plane of sky  $B_p$ . Without direct measurement of the full field strengths, the role magnetic fields play in star formation can only be assessed using indirect estimates of  $B_p$  (the Chandrasekhar-Fermi method as used by Lai et al. 2001) and some statistical arguments (Crutcher 1999).

Houde et al. (2002) proposed an interesting new approach to probe the orientation of magnetic fields. Houde et al. (2000a,b) show that in weakly ionized plasma, even under weak fields ( $\sim 10 \mu\text{G}$ ), the cyclotron interaction between the ions and the field can reduce the linewidth and suppress the high velocity wings in the ion spectra when compared to coexistent neutral spectra. Their HCN and  $\text{HCO}^+$  observations with the Caltech Submillimeter Observatory (CSO) show evidence of these predicted features. Because the ion-to-neutral linewidth ratio depends largely on the inclination angle of the magnetic fields (no cyclotron interaction along the field lines), the full strength and orientation of magnetic fields can be obtained by combining the observations of Zeeman splitting, polarimetry of dust continuum and/or CO emission, and the ion-to-neutral linewidth ratio. Houde et al. (2002) have constructed the 3-D field structure of M17 using this method.

However, it is difficult to interpret the differences in the velocity dispersions of the ion/neutral spectra unambiguously as being caused by the cyclotron interaction, if the beam is large enough to include the spectral line emissions from physically and chemically different components. The intrinsic difference between the velocity structure of the ions and neutrals will also contribute to the ion-to-neutral linewidth ratio. For example, if a velocity gradient exists in a large region with HCN, but  $\text{HCO}^+$  only coexists with HCN in a small part of this region, the HCN linewidth is naturally larger than the  $\text{HCO}^+$  linewidth. Therefore, it is important to obtain high spatial resolution spectral line maps to resolve the regions with widely different physical and chemical characteristics.

In this paper, we present the comparison between  $\text{H}^{13}\text{CN}$  and  $\text{H}^{13}\text{CO}^+$  spectra in DR21(OH) observed with the millimeter array of the Owens Valley Radio Observatory (OVRO). DR21(OH) is an excellent object to study the magnetic field structure, because it is in the early stage of massive star formation. DR21(OH) is one of the few sources with measured average line-of-sight magnetic field strength from CN Zeeman detections (Crutcher et al. 1999) and field directions in the plane of sky mapped with BIMA using both dust and CO polarimetry (Lai et al. 2003). Deriving the full strength and 3-D structure requires

knowledge of the inclination angle of the magnetic field to the line of sight, which can be obtained by measuring the ion-to-neutral linewidth ratio.

## 2. Observations and Results

The observations were made with the OVRO Millimeter Array at 3mm in the Compact, Low, and High resolution array configurations between October 2002 and May 2003. We obtained simultaneously spectral line images of HCN & HCO<sup>+</sup> and H<sup>13</sup>CN & H<sup>13</sup>CO<sup>+</sup>; <sup>13</sup>CS and N<sub>2</sub>H<sup>+</sup> were observed in the opposite sidebands. The synthesized beam is 6.4''×6.9'' for natural weighting and spectral resolutions are 0.434 km s<sup>-1</sup>. Among these images, the HCN and HCO<sup>+</sup> spectra show features of optically thick emission with strong self-absorption; N<sub>2</sub>H<sup>+</sup> has a very different spatial distribution compared to other species; H<sup>13</sup>CN, H<sup>13</sup>CO<sup>+</sup>, and <sup>13</sup>CS have a similar spatial distribution, but <sup>13</sup>CS has a different velocity structure from the other two. Therefore, H<sup>13</sup>CN and H<sup>13</sup>CO<sup>+</sup> are the only neutral/ion pair that can be used to examine the cyclotron effect in our data.

Figure 1 shows the 3mm continuum and the integrated flux of H<sup>13</sup>CN and H<sup>13</sup>CO<sup>+</sup>. The two compact cores in DR21(OH), MM1 and MM2, are resolved. H<sup>13</sup>CN and H<sup>13</sup>CO<sup>+</sup> both trace the dense cores very well. H<sup>13</sup>CO<sup>+</sup> is slightly more extended than H<sup>13</sup>CN, which is probably due to the lower critical density of H<sup>13</sup>CO<sup>+</sup>. Therefore, H<sup>13</sup>CN and H<sup>13</sup>CO<sup>+</sup> seem to occupy the same volume. Figure 2 shows the normalized H<sup>13</sup>CN and H<sup>13</sup>CO<sup>+</sup> spectra overlaid on their flux ratio map. Note that H<sup>13</sup>CN has three hyperfine lines with intensity ratios of 1:5:3 for the optically thin case. The spectra show that DR21(OH) contains two dominant velocity components – one at  $\sim -5$  km s<sup>-1</sup> and the other at  $\sim -1$  km s<sup>-1</sup>, which are likely to be associated with MM1 and MM2, respectively. At the positions between MM1 and MM2, the spectra are more complex and may contain an absorption feature at  $\sim -2.5$  km s<sup>-1</sup>. Overall, the spectra of H<sup>13</sup>CN and H<sup>13</sup>CO<sup>+</sup> trace each other well, which is strong evidence for the coexistence of H<sup>13</sup>CN and H<sup>13</sup>CO<sup>+</sup>, as also suggested by their spatial intensity correlation.

A difference in the ion/neutral linewidth can arise in some cases from chemical inhomogeneity, especially, if multiple velocity features are present. In Figure 2 we show the distribution of the H<sup>13</sup>CN-to-H<sup>13</sup>CO<sup>+</sup> flux ratio (in greyscale) which is a measure of the chemical differentiation in the core. We can safely discard the effects of chemical differentiation by excluding regions where the flux ratio changes appreciably over the small spatial scale sizes of the OVRO beam. However, chemical differentiation alone will not always cause linewidth differences. The velocity structure of the region also needs to be considered. For example, if the velocity structure is uniform across the cores such that the shape and the

central velocity of the spectra stay the same, any local variation in the ion-to-neutral flux ratio will result in a weighting factor that affects only the line intensities, not the ion-to-neutral linewidth ratios for the whole core. However, in DR21(OH) at least two velocity components are detected and therefore, it is critical to isolate the regions with different dynamics when interpreting the ion-to-neutral linewidth ratio as the cyclotron effect. We see a large variation in their flux ratio (by factors of 0.5 to 4) over the entire region, but it appears to be smooth except near the southwest parts of the core. In the eastern parts of the core the variation in the flux ratio is small, and the fully resolved velocity structure is dominated by a single feature. Thus, in this region of DR21(OH), we are able to minimize any contribution to the ion/neutral linewidth differences arising from chemical inhomogeneity. In our analysis we do not include the southwest region where rapid and significant variation of ion-to-neutral flux ratio is observed. Furthermore, the ion/neutral spectra in the southwest region have low S/N.

In the eastern part of MM1 where the  $-5 \text{ km s}^{-1}$  component dominates and the spectral line shapes are better defined, we can see that  $\text{H}^{13}\text{CO}^+$  is slightly narrower than  $\text{H}^{13}\text{CN}$ . To eliminate the complication of the  $\text{H}^{13}\text{CN}$  hyperfine lines, we simulate  $\text{H}^{13}\text{CN}$  spectra with all three hyperfine lines using the  $\text{H}^{13}\text{CO}^+$  as a ‘template’. For the case of a single velocity component, if the linewidth of  $\text{H}^{13}\text{CN}$  is smaller than half of the velocity separations between hyperfine lines, the difference spectrum between the observed  $\text{H}^{13}\text{CN}$  and that simulated from  $\text{H}^{13}\text{CO}^+$  is largely free from the confusion caused by the hyperfine components and thus is a useful measure of the cyclotron interaction. If indeed  $\text{H}^{13}\text{CN}$  has larger linewidths than  $\text{H}^{13}\text{CO}^+$ , the difference spectra will have two positive peaks near the wings of the line profile as demonstrated in Figure 2d. As the line shapes of  $\text{H}^{13}\text{CN}$  and  $\text{H}^{13}\text{CO}^+$  are approximately Gaussians, the integration of the difference spectra over the extent of the main hyperfine component gives a measure of the difference of the dispersions in the spectra.

$$\int (I_n - I_i) dv = \sqrt{2\pi}(\sigma_n - \sigma_i), \quad (1)$$

where  $I_n$  and  $I_i$  are the normalized  $\text{H}^{13}\text{CN}$  and  $\text{H}^{13}\text{CO}^+$  spectra and  $\sigma_n$  and  $\sigma_i$  are the dispersions of  $\text{H}^{13}\text{CN}$  and  $\text{H}^{13}\text{CO}^+$ , respectively. Figure 3a shows the map of  $(\sigma_n - \sigma_i)$  which is calculated by integrating the difference spectra over the  $-5 \text{ km s}^{-1}$  component ( $v_{\text{LSR}} = -9$  to  $-2.5 \text{ km s}^{-1}$ ). These  $(\sigma_n - \sigma_i)$  estimated using Eq(1) are in good agreement (within 10%) with those obtained by fitting Gaussians to the observed  $\text{H}^{13}\text{CN}$  and  $\text{H}^{13}\text{CO}^+$  line profiles at  $(+10'', +5'')$ . The signal-to-noise ratio (S/N) of  $(\sigma_n - \sigma_i)$  is presented in Figure 3b. We use  $(\sigma_n - \sigma_i)$  and  $\sigma_i$  measured from  $\text{H}^{13}\text{CO}^+$  spectra to derive  $(\sigma_i/\sigma_n)$  in Figure 3c. It is evident from the results shown in Figure 3 that in the eastern side of MM1 the ion linewidth is smaller than the neutral linewidth. We do not present similar analysis for the  $-1 \text{ km s}^{-1}$  component, because of the low S/N of  $(\sigma_n - \sigma_i)$ .

### 3. Discussion

The interferometer observations with OVRO have the advantage to resolve the velocity and chemical structures in the DR21(OH) core with high spatial resolution. In the eastern parts of DR21(OH) our observations show that  $\text{H}^{13}\text{CN}$  and  $\text{H}^{13}\text{CO}^+$  coexist over  $15'' \times 10''$  in a single velocity feature and confirm that the ion line is indeed narrower than the neutral line. We use the ion-to-neutral linewidth ratio ( $\sigma_i/\sigma_n$ ) shown in Figure 3c to infer the inclination angle of the magnetic field to the line of sight ( $\alpha$ ) according to Equation (11) of Houde et al. (2002). To derive the value of ( $\alpha$ ) using the ion/neutral linewidth ratio we require knowledge of the gas motions within the core. Houde et al. consider the cases with neutral flow collimation widths,  $\Delta\theta$ , ( $\Delta\theta = 90^\circ$  means no collimation as in a purely turbulent case). For a given value of ( $\sigma_i/\sigma_n$ ) a range of values for  $\alpha$  are possible depending on the values for flow collimation widths (see Figure 4 in Houde et al.). For example the average ion-to-neutral linewidth ratio, ( $\sigma_i/\sigma_n$ ) of 0.82 will correspond to an inclination angle  $\alpha = 76^\circ$ ,  $60^\circ$  and  $36^\circ$  for  $\Delta\theta=20^\circ$ ,  $45^\circ$  and  $90^\circ$  respectively. The dependence of the estimates for  $\alpha$  on  $\Delta\theta$  is less critical for  $\Delta\theta \sim 90^\circ$ , a case when turbulent motions dominate over collimated flows. Although MM1 in DR21(OH) does power high velocity CO outflows (Lai et al. 2003), there is no evidence that the spectra of ions and neutrals observed at the rest velocity of the cores are contaminated by collimated flows. Therefore, to derive the magnetic field inclination, we have ignored collimated flows and we assume the gas is fully turbulent ( $\Delta\theta = 90^\circ$ ). Figure 4 shows the inclination angle  $\alpha$  ranges from  $30^\circ$  in the northern part of MM1 to  $42^\circ$  in the south, and the uncertainty in  $\alpha$  is  $\sim 4-8^\circ$ . The variation in  $\alpha$  is small ( $12^\circ$ ) and is comparable to the variation of the overlaid  $B_p$  vectors derived from the dust polarization (black) and CO polarization (white). Therefore, the magnetic field directions seem to be approximately uniform across the MM1 region. The average line-of-sight magnetic field strength in MM1  $\sim -0.36 \pm 0.10$  mG as measured by CN Zeeman observations (Crutcher et al. 1999). With the average  $\alpha = 36^\circ$ , the field strength in the plane of sky ( $B_p$ ) is  $0.25 \pm 0.07$  mG, and the full magnetic field strength is  $0.44 \pm 0.12$  mG. The direction of the field is out of the plane of the sky towards the observer at an angle of  $36^\circ$  to the line of sight, and its projection on the sky is at a position angle  $-75^\circ$ .

Lai et al. (2003) estimate  $B_p \sim 0.9$  mG for MM1 from the observed dispersion in the CO polarization position angles using the Chandrasekhar-Fermi formula. This value is a factor of 3 larger than what is derived from the cyclotron interaction data presented here. This discrepancy could be partly due to the low values for the dispersion caused by the smoothing of polarization by the finite beam size of the BIMA observations. Also, the ‘calibration factor’ of the Chandrasekhar-Fermi formula (0.5) used by Lai et al. (2003) is an average value of clouds in numerical simulations (Ostriker, Gammie, & Stone 2001), which may not be a proper value DR21(OH).

With the knowledge of the full magnetic field strength, we can evaluate the role that magnetic fields play for star formation in MM1. First, we can calculate the mass-to-magnetic flux ratio from  $M/\Phi_B = 1.0 \times 10^{-20} N(H_2)/|B|$  in units of the critical mass-to-flux ratio (Crutcher 1999), where  $N(H_2)$  is the column density in  $\text{cm}^{-2}$  and  $|B|$  is the field strength in  $\mu\text{G}$ . With  $N(H_2) = 2 \times 10^{23} \text{ cm}^{-2}$  and  $B=0.44 \text{ mG}$ ,  $M/\Phi_B = 4.5$ . Therefore, MM1 is clearly magnetically supercritical. However, turbulence seems to provide dominant support. The  $\text{H}^{13}\text{CO}^+$  linewidth ( $\sim 2.2 \text{ km s}^{-1}$ ) is much larger than its thermal linewidth for  $T_k=50 \text{ K}$  ( $0.3 \text{ km s}^{-1}$ ), indicating strong turbulence in DR21(OH). The relative importance of magnetic, thermal, and turbulent support can be evaluated by comparing their energy to the gravitational energy. We find that in MM1 the magnetic-to-gravitational energy ratio is 0.05, the thermal-to-gravitational energy ratio is 0.16, and the turbulent-to-gravitational energy ratio is 0.66. Therefore, turbulence provides the dominant support in MM1. Although our conclusion on the status of MM1 is similar to what has been suggested by Crutcher et al. (1999) with statistical argument for the full magnetic field strength, our results exclude the possibility of the magnetic field dominance which may be true only if the field orientation in 3-D is very close to the plane of the sky.

We thank the referee for helpful suggestions. This research was conducted at the Jet Propulsion Laboratory, California Institute of Technology, with support from the National Aeronautics and Space Administration, while SPL held a National Research Council Resident Research Associateship at JPL. The OVRO Millimeter Array is supported by NSF grant AST-99-81546.

## REFERENCES

- Crutcher, R. M. 1999, *ApJ*, 520, 706
- Crutcher, R. M., Troland, T. H., Lazareff, B., Paubert, G., & Kazès, I. 1999, *ApJL*, 514, L121
- Dotson, J. L., Davidson, J., Dowell, C. D., Schleuning, D. A., & Hildebrand, R. H. 2000, *ApJS*, 128, 335
- Girart, J. M., Crutcher, R. M., & Rao, R. 1999, *ApJL*, 525, L109
- Houde, M., Bastien, P., Peng, R., Phillips, T. G., & Yoshida, H. 2000a, *ApJ*, 536, 857
- Houde, M., Peng, R., Phillips, T. G., Bastien, P., & Yoshida, H. 2000b, *ApJ*, 537, 245

Houde, M., Phillips, T. G., Bastien, P., Peng, R., & Yoshida, H. 2001, ApJ, 547, 311

Houde, M. et al. 2002, ApJ, 569, 803

Lai, S.-P., Crutcher, R. M., Girart, J. M., & Rao, R. 2001, ApJ, 561, 864

Lai, S.-P., Crutcher, R. M., Girart, J. M., & Rao, R. 2002, ApJ, 566, 925

Lai, S.-P., Crutcher, R. M., & Girart, J. M. 2003, ApJ, in press

Ostriker, E. C., Stone, J. M., & Gammie, C. F. 2001, ApJ, 546, 980

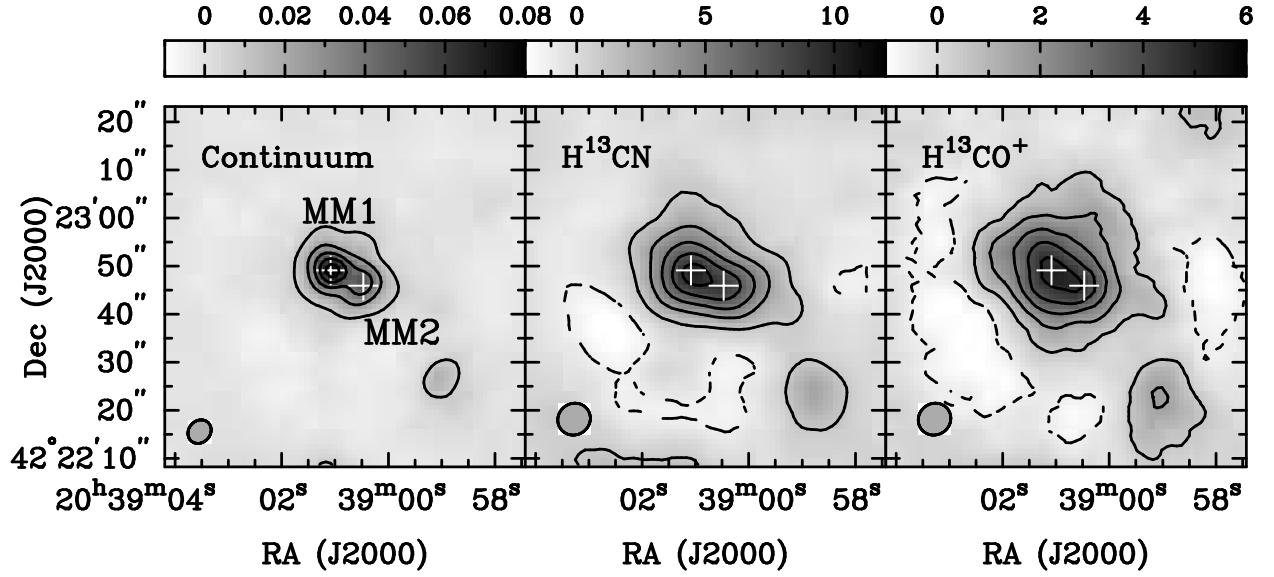


Fig. 1.— The 3mm dust continuum and the velocity integrated intensity maps of  $\text{H}^{13}\text{CN}$  and  $\text{H}^{13}\text{CO}^+$ . The lowest contour and the interval are at 10% and 20%, respectively, of the peak intensities.



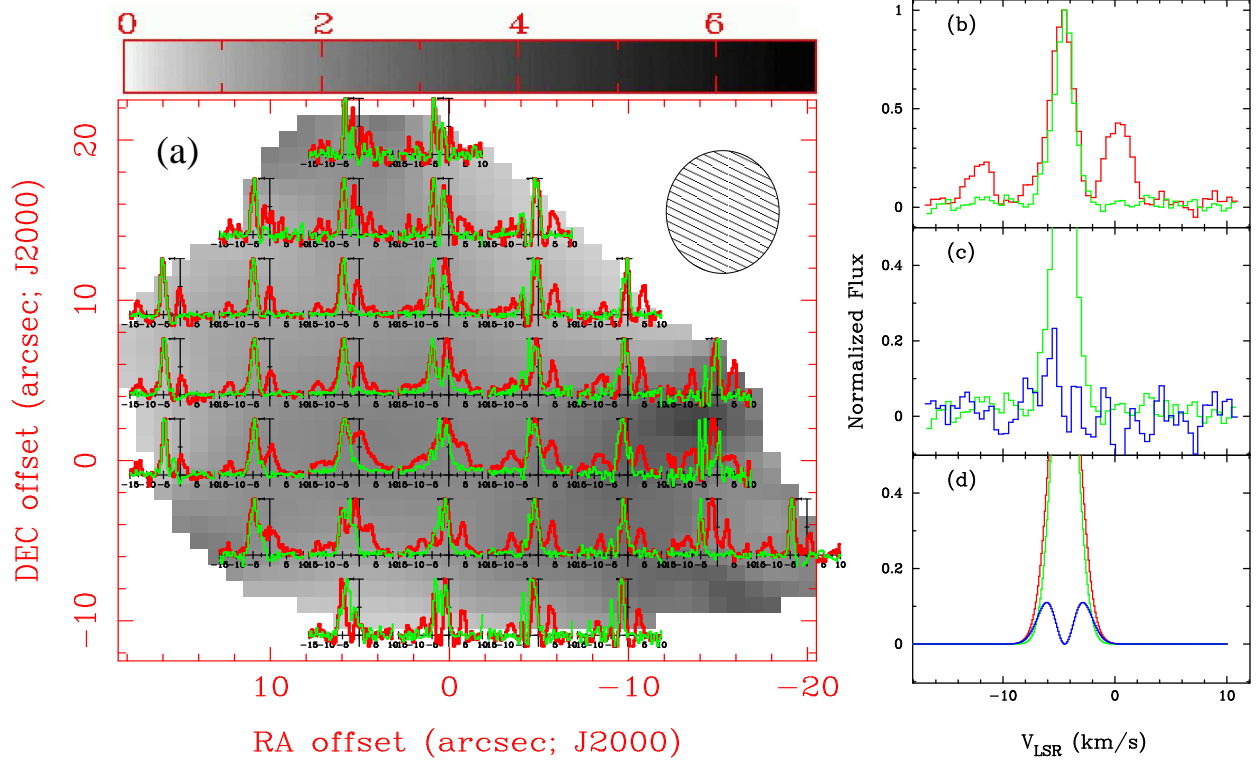


Fig. 2.— Spectra of Ions and Neutrals. **(a)** Normalized H<sup>13</sup>CN (red) and H<sup>13</sup>CO<sup>+</sup> (green) spectra overlaid on H<sup>13</sup>CN-to-H<sup>13</sup>CO<sup>+</sup> flux ratio (greyscale). The beam size is indicated. **(b)** H<sup>13</sup>CN (red) and H<sup>13</sup>CO<sup>+</sup> (green) spectra at offset position (+10'', +5''). **(c)** Difference spectrum at this position between observed H<sup>13</sup>CN and simulated H<sup>13</sup>CN (using H<sup>13</sup>CO<sup>+</sup> profile as a template - see §2) is shown in blue. H<sup>13</sup>CO<sup>+</sup> spectrum (green) is shown for comparison. **(d)** Difference spectrum for model Gaussian spectra with  $(\sigma_i/\sigma_n) = 0.86$ , equivalent to that for the (+10'', +5'') position.

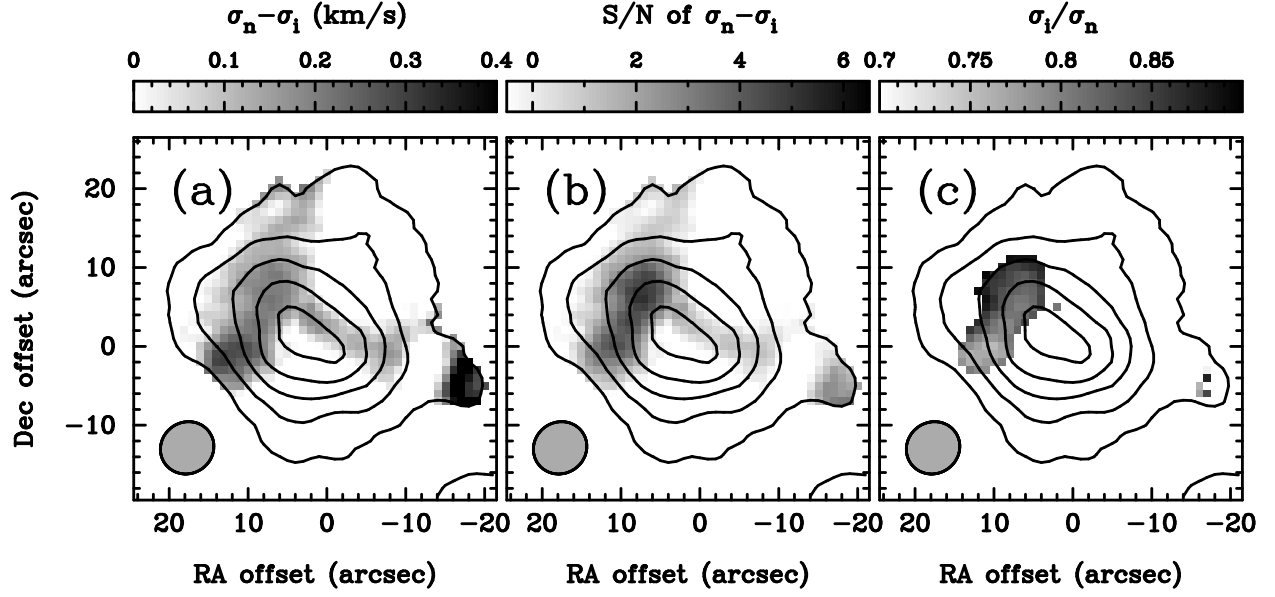


Fig. 3.— Greyscale maps of ion/neutral linewidth differences overlaid on contours of  $\text{H}^{13}\text{CO}^+$  integrated flux at 10%, 30%, 50%, 70%, and 90% levels. **(a)** Difference of  $\text{H}^{13}\text{CN}$  and  $\text{H}^{13}\text{CO}^+$  line dispersion ( $\sigma_n - \sigma_i$ ). **(b)** Signal-to-noise ratio of ( $\sigma_n - \sigma_i$ ). **(c)** Linewidth ratio ( $\sigma_i / \sigma_n$ ) for S/N of ( $\sigma_n - \sigma_i$ ) > 2.5.

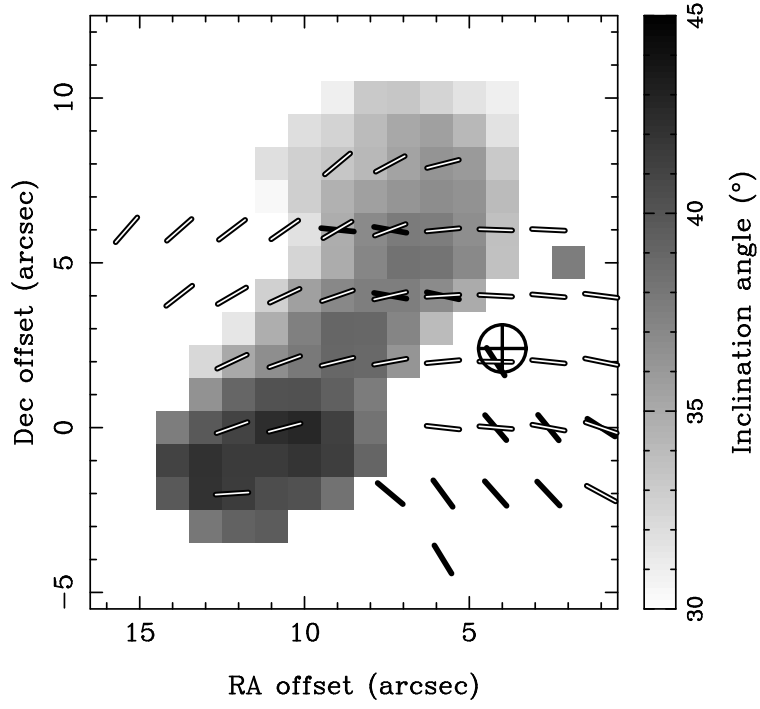


Fig. 4.— Magnetic Field structure in DR21(OH) MM1 core. The greyscale shows the inclination angle of the magnetic field to the line of sight ( $\alpha$ ) varying from  $30^\circ$  to  $42^\circ$ . The vectors represent  $B_p$  orientation inferred from dust (black) and CO (white) polarization.  $\oplus$  represents the CN Zeeman measurement of line-of-sight component,  $\sim 0.36$  mG towards observer.